Wear 267 (2009) 860–866

Contents lists available at ScienceDirect

Wear

journal homepage: www.elsevier.com/locate/wear

Tribocorrosion behaviour of DLC-coated 316L stainless steel

M. Azzi[a,b], M. Paquette[b], J.A. Szpunar[a], J.E. Klemberg-Sapieha[b], L. Martinu[b,*]

[a] Department of Mining and Materials Engineering, McGill University, Montreal, QC, Canada, H3A 2B2
[b] Department of Engineering Physics, Ecole Polytechnique, Montreal, QC, Canada, H3C 3A7

ARTICLE INFO

Article history:
Received 18 September 2008
Received in revised form 4 February 2009
Accepted 4 February 2009

Keywords:
Tribocorrosion
316L
Wear
DLC
a-SiN_x:H
EIS
Corrosion

ABSTRACT

In the present work, we systematically investigate the tribocorrosion behaviour of diamond-like carbon (DLC) films on 316L stainless steel substrates in the context of their biomedical applications. Two different bond layers at the interface were particularly studied, namely the plasma nitrided layer and the plasma deposited amorphous hydrogenated silicon nitride (a-SiN_x:H). Tribocorrosion tests were performed using a ball-on-flat tribometer where the sliding contact is fully immersed in NaCl 1 wt.% solution. The sample was connected to a potentiostat: it served as a working electrode and its open circuit potential (OCP) was monitored before, during, and after sliding. Electrochemical impedance spectroscopy (EIS) was applied to characterize the electrochemical behaviour of the surfaces before and after rubbing. The OCP measured during sliding was shown to depend on the properties of the protective layer; a decrease in the OCP indicates delamination of the protective layer and subsequent exposure of the substrate to the electrolyte. We found that the DLC coating with the nitrided bond layer delaminated from the wear track within 50 cycles of sliding, while it resisted the entire tribocorrosion test (1800 cycles) without failure when the a-SiN_x:H bond layer was applied. The EIS results are interpreted in terms of appropriate equivalent circuits. It is shown that the a-SiN_x:H bond layer significantly increases the corrosion resistance by acting as a corrosion barrier, while the DLC coating assures high wear resistance and low friction. The polarization resistance of DLC-coated 316L with the a-SiN_x:H bond layer was found to be 3.76 GΩ cm^2 compared to 27.5 MΩ cm^2 for the same DLC coating without a-SiN_x:H.

1. Introduction

Tribocorrosion is a term which describes the degradation of materials that results from the combined action of wear and corrosion [1,2]. Examples include degradation of articulation prosthesis and dental fillers, accelerated corrosion of steel conveyors exposed to ambient air of high relative humidity, erosion-corrosion of slurry pipes, and numerous others. When corrosion and wear are simultaneously involved, their synergistic action significantly deteriorates the performance of the materials in contact.

Over the past years, a number of authors investigated the tribocorrosion behaviour of engineering substrates. Mischler and co-workers [1,2] studied the effect of applied voltage on the wear mechanisms of Fe–17Cr stainless steel and carbon steel. Ponthiaux et al. [3] investigated the tribocorrosion behaviour of 316L stainless steel. Barril et al. [4] used the potentiostatic polarization technique to investigate the fretting corrosion behavior of Ti–6Al–4V in 0.9 wt% sodium chloride solutions.

In orthopaedic applications, artificial joints (e.g., hip and knee prostheses) include bearing surfaces where the material is subjected to sliding wear. The surfaces in contact are immersed in the body fluid, and therefore, corrosion may also be a concern. For such application, metals and alloys must possess high tribocorrosion resistance. Particles generated from wear of prosthetic implants induce inflammatory reactions that provoke the release of inflammatory mediators from macrophages [5]. It is well established that the cellular response to wear debris depends, among other factors, on the number, shape, size, surface area, and materials chemistry of the particles [6,7].

In recent years, diamond-like carbon (DLC) films have been the subject of extensive investigations due to their potential of attaining a combination of highly desirable properties in the context of biomedical applications [8–14]. Their high hardness, low friction and wear, electrical insulation, chemical inertness and good biocompatibility make them ideal candidate as protective coatings in joints replacement [8].

DLC films are usually characterized by an sp^2–sp^3 hybridization ratio of approximately 0.4, and a hydrogen concentration in the range of 20–40 at.% [9]. Raveh et al. [10,11] studied the relationship between the structure of the DLC films and their mechanical and tribological properties. The authors reported that DLC films containing predominantly unbonded hydrogen can resist more severe conditions of sliding friction than those containing predominantly bonded hydrogen. Martinu et al. [12] showed that the addition of

* Corresponding author. Tel.: +1 514 340 5747; fax: +1 514 340 3218.
E-mail address: lmartinu@polymtl.ca (L. Martinu).

0043-1648/$ – see front matter © 2009 Elsevier B.V. All rights reserved.
doi:10.1016/j.wear.2009.02.006

Table 1
Experimental conditions of sample pre-treatment, nitriding, DLC and a-SiN_x:H deposition, and the corresponding hardness and Young's modulus.

Operation	Pressure (mTorr)	Gaseous mixture (sccm)	Bias voltage (V)	Process duration (min)	Hardness (GPa)	Young's modulus (GPa)
Ar sputter-cleaning	100	Ar (10)	−800	15	6	220
Nitriding	100	N_2 (50)	−500	180	15	220
a-SiN_x:H deposition	100	SiH_4 (6.6), N_2 (20), Ar (30)	−400	10	17	160
DLC deposition	100	CH_4 (40), Ar (10)	−500	30	18	140

argon to the hydrocarbon feed gas and the application of a combination of microwave and radio frequency power during plasma deposition substantially enhance gas phase processes such as dissociation of CH_4 and formation of the sp^3 component in the DLC, leading to a substantial decrease in the mechanical stress.

Another important factor that influences the protective character of DLC films is their adhesion to the substrate. Many authors pointed out the importance of the bond layers for enhanced adhesion of the DLC films. Snyders et al. [13] suggested a simple nitrided bond layer. They reported significantly improved adhesion and dry wear resistance of DLC on 316L stainless steel. Chandra and coworkers [14] successfully tested amorphous hydrogenated silicon (a-Si:H) bond layer on Ti–6Al–4V.

One should keep in mind that pores are often present, even in good quality DLC films [15]. In this context, electrochemical impedance spectroscopy (EIS) was shown to be a sensitive technique in detecting pores and defects even at the nano-scale [16–19]. In addition, different circuits were used to simulate the impedance spectra, incorporating elements representing microstuctural features such as open pores that allow the infiltration of the electrolyte through the film. Lillard et al. [20] used the EIS technique to study the breakdown mechanism of DLC-coated nickel in chloride solution. The authors reported the initiation of breakdown at the bottom of the pores inside the DLC film.

In this work, we systematically investigate the tribocorrosion behaviour of DLC-coated 316L stainless steel exposed to the Ringer's solution in the context of biomedical applications. Two different bond layers are studied, namely amorphous hydrogenated silicon nitride (a-SiN_x:H) and plasma nitrided layers. Electrochemical techniques such as open circuit potential (OCP) measurements and EIS are applied for the assessment of the corrosion resistance.

2. Experimental methodology

2.1. Coating deposition

DLC coatings were deposited on 316L stainless steel substrates (25 mm × 25 mm × 1.2 mm) using a turbo-molecularly pumped radio frequency (13.56 MHz) PECVD system, equipped with a 15 cm diameter electrode where a self-induced DC bias voltage, V_B, develops. Two different methods for interface engineering between the 316L substrate and the DLC film were used in this study: (1) nitriding of the stainless steel surface, and (2) deposition of amorphous hydrogenated silicon nitride bond layer.

The 316L substrates were mechanically polished using 1 μm alumina suspension. After polishing the specimens were ultrasonically cleaned in acetone (15 min) and isopropanol (15 min), and then introduced into the deposition chamber. Prior to nitriding or deposition, the substrates were cleaned with Ar plasma sputtering for 15 min to remove the native oxide eventually formed after polishing. The experimental conditions of the substrate pre-treatment, the interface engineering and the DLC film deposition are summarized in Table 1, as well as the mechanical properties obtained from the nano-indentation measurements.

2.2. Tribocorrosion test

Tribocorrosion experiments were performed using a linear reciprocating ball-on-flat tribometer described in Ref. [21]. During the tests, a 3/16″ (4.75 mm) diameter alumina ball rubs on the specimen surface immersed in the test solution. The sample served as the working electrode and its potential was controlled using Autolab PGSTAT302 potentiostat equipped with a frequency response analyser. The counter electrode was made of coiled platinum, and the standard calomel electrode SCE (+241 mV versus standard hydrogen electrode) was used as a reference for the potential measurements.

Sliding tests were carried out with 9 N normal force applied using a compression spring. This corresponds to a maximum Hertzian contact pressure of 1.18 GPa, calculated based on the contact between the alumina ball and the 316L flat surface. The stroke length was 10 mm, and the sliding frequency was 1 Hz. Ringer's solution of pH ≈6.6 was used as an electrolyte: its composition was 9 g/l NaCl, 0.4 g/l KCl, 0.17 g/l $CaCl_2$ and 2.1 g/l $NaHCO_3$ in distilled water.

The sequence of operations during the tribocorrosion test is schematically illustrated in Fig. 1 that shows an evolution of the OCP. First, the sample was immersed in the Ringer's solution for

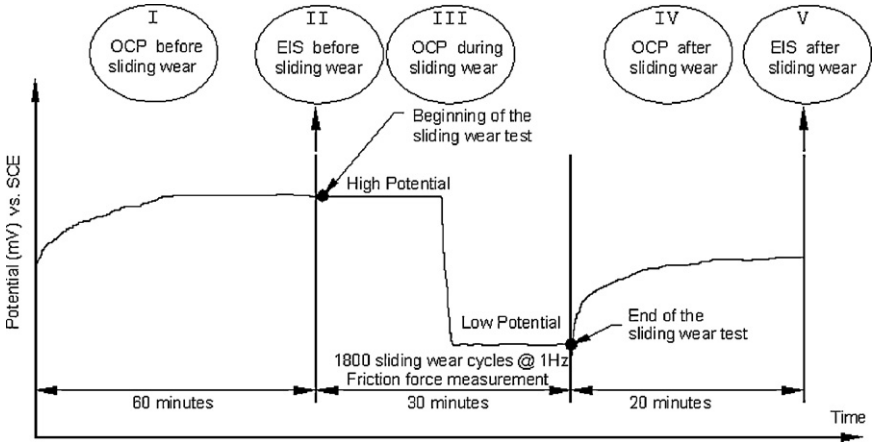

Fig. 1. Sequence of operations during the tribocorrosion test illustrated by the OCP evolution.

1 h in order to reach a stable potential (Region I). Next, EIS was performed to characterize the electrochemical behaviour of the surface before sliding wear (Region II). Subsequently, the alumina ball was loaded on the sample surface and the sliding test was initiated. The sliding was stopped after 1800 cycles. During and after the sliding wear test, the OCP was continuously monitored (Regions III and IV). Finally, EIS was performed to characterize the electrochemical behaviour of the surface after sliding (Region V). The EIS spectra were acquired over the frequency range from 10^5 Hz to 10^{-2} Hz, at OCP, with an AC amplitude of 10 mV.

Tribocorrosion behaviour of the bare 316L stainless steel substrates (SS), DLC-coated 316L with nitrided (3 h) bond layer (SS/N3h/DLC), and of the DLC-coated 316L with the a-SiN_x:H bond layer (SS/a-SiN_x:H/DLC) was investigated. The tribocorrosion experiments were repeated three times for the same surface condition to validate the results. SS, SS/N3h/DLC and SS/a-SiN_x:H/DLC notations will be used in the rest of this paper to represent the above mentioned samples.

2.3. Surface characterization

Field emission scanning electron microscope (FESEM, Philips XL30) equipped with an energy dispersive spectrometer (EDS) was used to perform cross-section analysis of the coated substrates and to characterize the worn surfaces. A Rigaku Rotaflex X-ray diffractometer (XRD) was used to characterize the crystal structure of the deposited films. XRD spectra were acquired at a grazing angle of 1.5°, using CuKα radiation of 1.54 nm wavelength, under 40 kV voltage and 40 mA current. Chemical compositions of the DLC and a-SiN_x:H films were measured by the elastic recoil detection (ERD) technique in the time-of-flight regime [10].

3. Results and discussion

3.1. Characterization of the as-deposited coatings

Fig. 2 shows the SEM cross-section micrographs of SS/N3h/DLC and SS/a-SiN_x:H/DLC. For SS/a-SiN_x:H/DLC, the thicknesses of the a-SiN_x:H and DLC layers were approximately 350 nm and 650 nm, respectively. For SS/N3h/DLC, the thickness of the DLC film was also about 650 nm. The white particles shown in Fig. 2(a) are polishing solution residues. Previous study of the nitrided layer [13] showed that the nitriding process at these conditions results in the formation of a relatively thick (1–2 μm), hard (15 GPa) metal nitride layer at the stainless steel surface. Chemical compositions determined by ERD of the DLC and a-SiN_x:H films are presented in Table 2.

Table 2
Chemical composition of the DLC and a-SiN_x:H films measured by ERD.

	C (at.%)	Si (at.%)	N (at.%)	H (at.%)
DLC	85	–	–	15
a-SiN_x:H	–	35	48	17

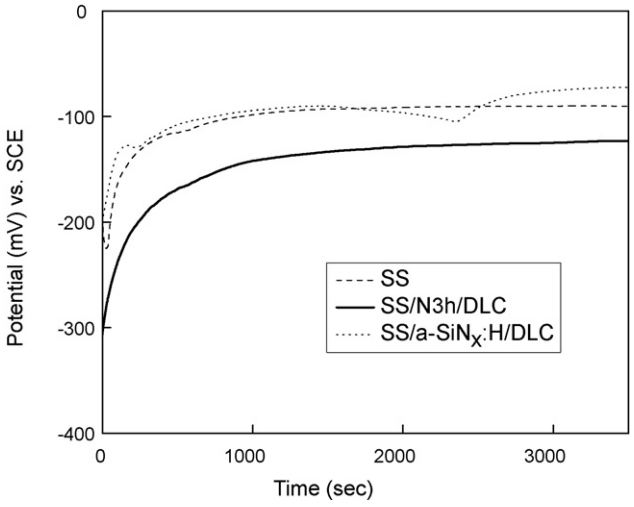

Fig. 3. OCP measurements before sliding of SS, SS/N3h/DLC, and SS/a-SiN_x:H/DLC in Ringer's solution.

XRD analysis has shown that both a-SiN_x:H and DLC layers are amorphous since no diffraction peaks were observed in the spectra.

3.2. Open circuit potential measurements

3.2.1. OCP before sliding

The OCP evolutions during the first hour of immersion of SS, SS/N3h/DLC, and SS/a-SiN_x:H/DLC in Ringer's solution are presented in Fig. 3. For all samples, the OCP increased and stabilized after 1 h, indicating a stable electrochemical condition at the surface. The OCP stabilized at −90 mV for SS, −125 mV for SS/N3h/DLC, and −70 mV for SS/a-SiN_x:H/DLC.

3.2.2. OCP during and after sliding

The OCP measurements during and after sliding of SS, SS/N3h/DLC, SS/a-SiN_x:H/DLC, and SS/a-SiN_x:H are shown in Fig. 4. For SS, a sudden decrease of the OCP was observed when rubbing started. The potential dropped to approx. −400 mV, and was fluctuating in phase with the reciprocating motion of the alumina ball. When rubbing ceased, the OCP first steeply increased and then

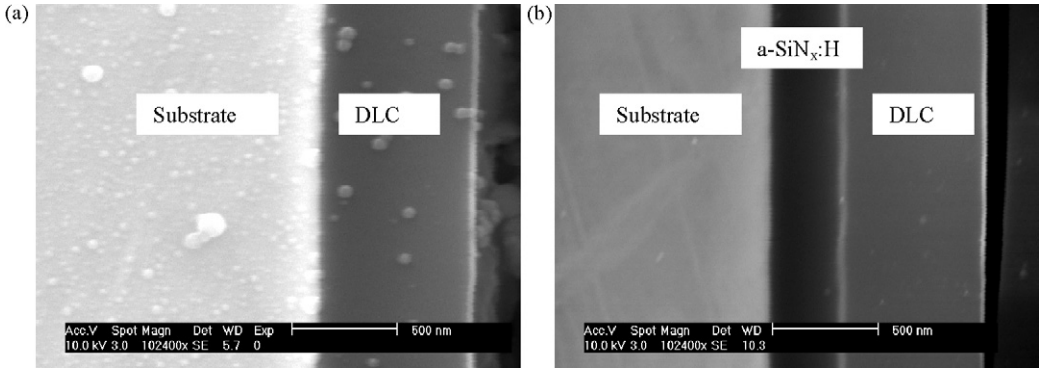

Fig. 2. SEM cross-sectional micrographs of (a) SS/N3h/DLC and (b) SS/a-SiN_x:H/DLC.

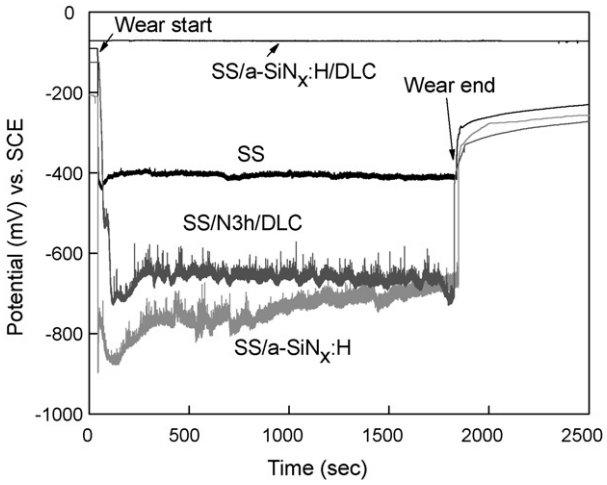

Fig. 4. OCP measurements during and after sliding test of SS, SS/N3h/DLC, SS/a-SiN_x:H and SS/a-SiN_x:H/DLC. Normal load: 9 N, frequency: 1 Hz.

progressively returned to a steady state value. During sliding the friction coefficient was about 0.3. For SS/N3h/DLC, the OCP dropped within the first 50 cycles of sliding to reach an average value of −650 mV. During the first few cycles, the friction coefficient was 0.08. Subsequently, it progressively increased to reach 0.3 after about 50 cycles. When sliding ceased, the evolution of OCP was similar to the one measured on SS; a steep increase followed by a progressive stabilization. In the case of SS/a-SiN_x:H/DLC, the OCP remained constant during and after sliding, and the fluctuations of the OCP during rubbing were small compared to the ones observed on the other samples. In addition, the friction coefficient was almost constant (0.08) throughout the entire sliding test. For SS/a-SiN_x:H, the OCP dropped, at the onset of rubbing, to an approx. value of −800 mV, and then increased when rubbing ceased.

The SEM images of the wear tracks of the different investigated samples are shown in Fig. 5. It is clearly seen that the DLC film delaminated from SS/N3h/DLC whereas on SS/a-SiN_x:H/DLC, the DLC film had no tendency to delaminate. For SS/a-SiN_x:H, the a-SiN_x:H film was completely removed from the wear track. In addition, a stainless steel transfer layer was observed on the alumina ball after all the tribocorrosion tests except the one performed on SS/a-SiN_x:H/DLC where the ball was found almost intact.

The sharp drop of the OCP observed at the onset of rubbing on SS is due to the removal of the oxide layer from the wear track area and the subsequent exposure of fresh active materials to the aqueous environment. Under these conditions, 316L stainless steel undergoes anodic dissolution followed by the formation of a passive oxide film on the surface according to the following reactions [22]:

$$M \rightarrow M^{n+} + ne^- \quad (1)$$

$$mM + nH_2O \rightarrow M_mO_n + H^+ + xe^-, \quad (2)$$

where M designates the metallic materials of the stainless steel, mainly Cr and Fe. The oxidation reactions (whether dissolution or oxide formation) take place in the wear track and generate electrons which must be consumed by the cathodic reaction in order for the oxidation reactions to proceed. The main cathodic reaction supporting the passivation reaction under these conditions is the reduction of the dissolved oxygen [22]:

$$O_2 + 2H_2O + 4e^- \rightarrow 4OH^- \quad (3)$$

Ponthiaux et al. [3] measured the OCP of 316 stainless steel substrate immersed in aerated 0.5 M sulphuric acid and rubbing against an alumina ball counterpart. They reported an OCP of approximately −800 mV vs. SCE during sliding compared to −400 mV vs. SCE in our case. The difference can be explained by the cathodic-to-anodic (CTA) ratio during sliding. In our tests, the total exposed area was 283.5 mm^2 and the wear track area was only 3 mm^2 (300 μm × 10 mm), as shown in Fig. 5(a). This results in a CTA ratio of 93, which is very high compared to the CTA in the Ponthiaux's experiments where a large part of the area outside the wear track was insulated with cataphoretic paint to reduce the cathodic reaction activities. Berradja et al. [23] studied the fretting behaviour of 304 stainless steel; they also reported a decrease of the potential at the onset of fretting experiments, and referred this drop to the exposure of the fresh active material to the environment. They measured only −200 mV vs. SCE since the depassivated area in the

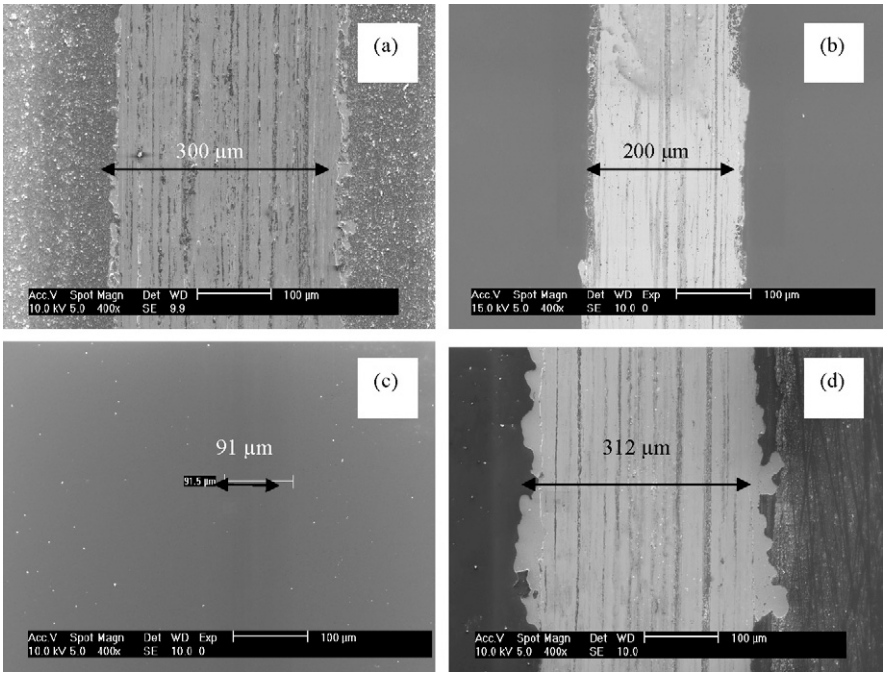

Fig. 5. SEM images of the wear tracks after 1800 cycles of sliding on (a) SS, (b) SS/N3h/DLC, (c) SS/a-SiN_x:H/DLC, and (d) SS/a-SiN_x:H.

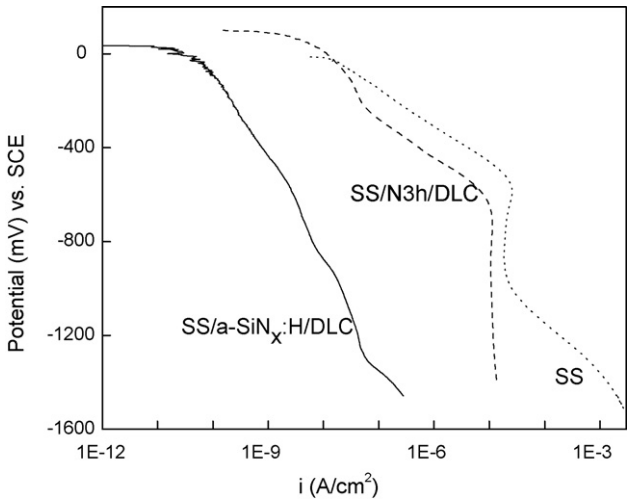

Fig. 6. Cathodic polarization curves of SS, SS/N3h/DLC and SS/a-SiN$_x$:H/DLC in Ringer's solution.

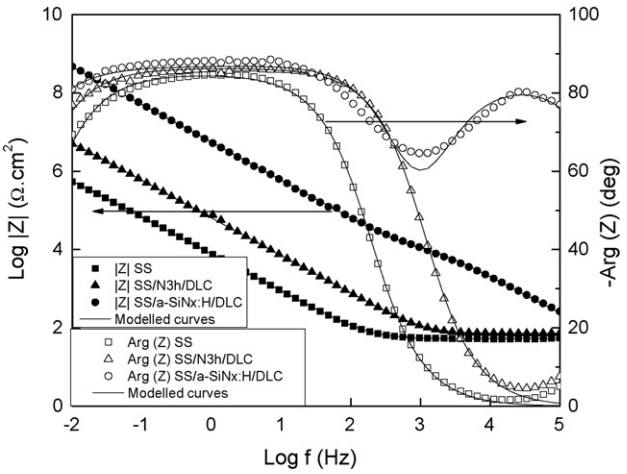

Fig. 7. EIS spectra and modelled curves of SS, SS/N3h/DLC and SS/a-SiN$_x$:H/DLC after 1 h immersion in Ringer's solution.

fretting experiment was very small compared to the sliding wear test.

For SS/N3h/DLC, the drop in the OCP indicates that the coating was completely removed after 50 cycles of sliding to leave behind a fresh active material in the wear track exposed to the electrolyte. However, the average OCP during sliding was relatively low (−650 mV) compared to the one measured on SS (−400 mV). This is due to the fact that the cathodic reaction rate was lowered by the presence of the DLC film on the unworn area. Indeed, the cathodic polarization curves of SS, SS/N3h/DLC and SS/a-SiN$_x$:H/DLC, presented in Fig. 6, show that the cathodic current density, i (A/cm^2), of the DLC-coated 316L is lower than the one of SS. For example, at −400 mV, the current densities were 4×10^{-6} A/cm^2, 5×10^{-7} A/cm^2, and 8×10^{-10} A/cm^2 for SS, SS/N3h/DLC, and SS/a-SiN$_x$:H/DLC, respectively. In addition, these curves show that the a-SiN$_x$:H film significantly reduces the rate of the cathodic reaction, and therefore explains the low value of the OCP measured on SS/a-SiN$_x$:H during the sliding test.

Snyders et al. [13] conducted dry sliding tests on the same SS/N3h/DLC samples, deposited in the same reactor and under the same conditions. They reported a high wear resistance without delamination up to 22 N normal load, using the same counterface material. This completely different behaviours under dry and wet conditions clearly revealed the effect of corrosion processes on the wear resistance of DLC coating. Lillard et al. [20] reported that the corrosion reactions at the bottom of the pores are the first step in the breakdown of DLC coatings in chloride solution. This is believed to be the reason for the delamination of the DLC film during the sliding test in Ringer's solution, the solution infiltration through the pores in the DLC may weaken the DLC/metal interface and reduce the adhesion of the DLC film.

For SS/a-SiN$_x$:H/DLC, the coating did not delaminate from the wear track. This explains why the OCP was relatively high and did not drop during the sliding test. The a-SiN$_x$:H layer significantly reduced the charge transfer between the metallic substrate and the electrolyte, as it will be shown later in this work, by acting as a barrier layer between the substrate and the electrolyte. Therefore, it reduced the possibility of weakening the interface between the substrate and the film. The combination of a-SiN$_x$:H and DLC films was appropriate for the wet wear conditions: the first layer significantly reduces the corrosion rate, while the second layer, due to its high hardness, assures wear resistance and low friction, and protects the a-SiN$_x$:H from mechanical wear.

The increase of the OCP, when rubbing ceases, is due to the repassivation of the stainless steel material. It was reported [1–3] that in the absence of sliding wear the stainless steel surface repassivetes and the OCP increases.

3.3. Electrochemical impedance spectroscopy (EIS)

3.3.1. EIS before the sliding test

The EIS spectra of SS, SS/N3h/DLC, and SS/a-SiN$_x$:H/DLC after 1 h of immersion in Ringer's solution are shown in Fig. 7. The value of the impedance |Z| is plotted on the left y-axis and the phase shift Arg(Z) is plotted on the right y-axis. The Arg(Z) plot of SS/a-SiN$_x$:H/DLC is shifted towards high angles at high frequencies indicating a more capacitive response of the film. In addition, the impedance of SS/a-SiN$_x$:H/DLC is almost three orders of magnitude larger than the impedance of SS, while it

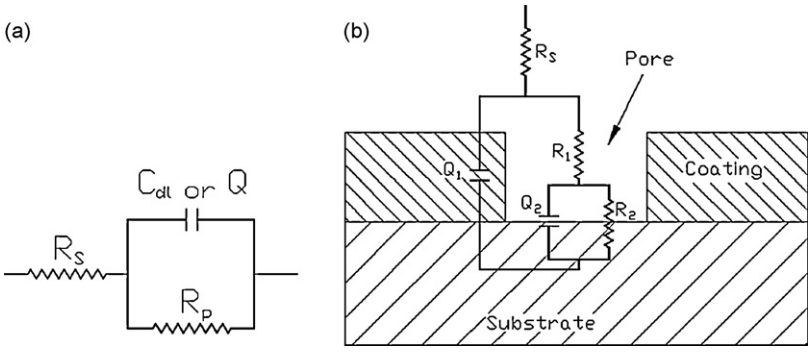

Fig. 8. Equivalent circuits used for EIS spectra simulation: (a) basic (Randle) circuit; (b) double capacitance circuit.

Table 3
Characteristics of the equivalent circuits derived from the modelling of EIS spectra.

Sample	R_s (Ω cm^2)	Q_1 (Y_o) (F/cm^2)	Q_1 (n)	R_1 (Ω cm^2)	Q_2 (Y_o) (F/cm^2)	Q_2 (n)	R_2 (Ω cm^2)
SS	53	-	-	-	0.22×10^{-4}	0.94	1.81×10^6
SS/N3h/DLC	60	-	-	-	0.26×10^{-5}	0.96	27.5×10^6
SS/a-SiN$_x$:H/DLC	35	0.16×10^{-7}	0.93	20.3×10^3	0.14×10^{-7}	0.99	3.76×10^9

is only one order of magnitude larger for SS/N3h/DLC compared to SS.

The spectra of SS and SS/N3h/DLC are characterized by a one time-constant behaviour, and therefore can be modelled by a basic equivalent circuit, called Randle circuit (see Fig. 8(a)). Such circuit consists of the following elements: R_s corresponds to the solution resistance of the test electrolyte between the working electrode and the reference electrode, C_{dl} is the capacitance which represents the charge build-up at the interface between the sample surface and the electrolyte, and R_p is the polarization resistance. R_p is proportional to the corrosion resistance of the surface. As the corrosion process at an electrochemical interface is complicated, EIS modelling requires the use of complex circuit elements such as the constant phase element, Q, which is often used to replace the capacitor C. Its impedance is expressed as [24]:

$$Z_Q = \frac{1}{[Y_o(jw)^n]}, \quad (4)$$

where Y_o is the parameter of Q (Ω^{-1} sec^n cm^{-2} or F sec^{n-1} cm^{-2}), w is the angular frequency, and n is the empirical exponent of Q that always lies between -1 and 1 [24]. Depending on the value of exponent n, the physical meaning of Q can be related to pure capacitance ($n = 1$), pure resistor ($n = 0$), and pure inductance ($n = -1$). The deviation of the impedance from pure capacitor behaviour can be attributed to the inhomogeneity in the coating system and non-uniform diffusion [19].

The spectrum of SS/SiN/DLC is characterized by a two time-constant behaviour since two peaks are observed in the Arg(Z) plot; therefore, the Randle circuit could not be used for modelling. Many electrical circuits were proposed in the literature to model EIS spectra of coatings with two time-constant behaviour [25]. The most commonly used equivalent circuit is shown in Fig. 8(b). It contains two constant phase elements: Q_1 represents the charge/discharge process at the film/electrolyte interface, and Q_2 represents the charge/discharge process that occurs at the substrate/electrolyte interface; the latter one is the result of the infiltration of the electrolyte through the film's pores to reach the substrate. It was reported [16,19] that pores with few nanometers in size can allow infiltration of the electrolyte. The resistance of ionic transfer inside the pores is represented by R_1; higher R_1 values indicate a lower pores size. In the absence of physical pores, R_1 represents the resistance to ionic transfer through the coating. The polarization resistance is represented by R_2.

Using the above mentioned equivalent circuits, the experimental EIS spectra of SS, SS/N3h/DLC, and SS/a-SiN$_x$:H/DLC were modelled and the best-fit curves are presented in Fig. 7. The characteristics of the equivalent circuits are summarized in Table 3. For SS, R_p was found to be 1.81 MΩ cm^2. The value of n was close to unity (0.94) indicating that Q represents a non-ideal capacitor with a capacitance of 0.22×10^{-4} F/cm^2.

For SS/a-SiN$_x$:H/DLC, R_2 was very high (3.76 GΩ cm^2), indicating excellent corrosion resistance of this coating. R_1 was found to be 20.3 kΩ cm^2, compared to 35 Ω cm^2 for the bulk solution. This reflects high resistance against the infiltration of the liquid through the film to reach the substrate. Since n_1 and n_2 were close to unity, Q_1 and Q_2 could be, as suggested, considered as capacitance. The low value of Q_1 could be related to the relatively thick a-SiN$_x$:H/DLC coating (1 μm) compared to the oxide film (few nanometers thick) formed on the bare substrate. The low value of Q_2 indicates low area of contact between the substrate and the electrolyte.

For SS/N3h/DLC, R_p was 27.5 MΩ cm^2 compared to 1.81 MΩ cm^2 for SS. This shows that the DLC film improves the corrosion resistance of the 316L surface. It also shows that the high resistance found in the case of SS/a-SiN$_x$:H/DLC is mainly due to the presence of a-SiN$_x$:H layer and not to the DLC film.

3.3.2. EIS after the sliding test

Before the sliding test, the surface area exposed to the electrolyte was homogeneous, and therefore it was possible to normalize the EIS simulation results for the surface area. After the wear test, the exposed surface consisted of two areas: the worn area (inside the wear track) and the unworn area (outside the wear track). Consequently, the EIS simulation results could not be normalized for the exposed area.

For SS, R_p was 177 kΩ compared to 640 kΩ ($1.81 \times 10^6/2.83$) before sliding. This difference indicates that the passive film formed in the active area of the wear track, 20 min after the end of sliding, has not yet regained its initial thickness and protective properties. Indeed, after stabilization of the worn sample for 24 h in the solution, EIS was performed and the results showed that R_p of the total area was very close to R_p calculated before sliding.

For SS/N3h/DLC, R_p was 319 kΩ after sliding compared to 9.75 MΩ before sliding. This significant decrease is due to the removal of the DLC coating from the wear track and the formation of new passive layer.

The EIS spectra of SS/a-SiN$_x$:H/DLC measured before and after sliding were very similar, indicating that the protective properties of a-SiN$_x$:H/DLC coating were not affected by the sliding, underlining its excellent tribocorrosion properties.

4. Summary

In this study, the effect of the bond layer on the tribocorrosion behaviour of DLC-coated 316L stainless steel was systematically evaluated. The nitrided bond layer shows a significant improvement of the dry wear resistance of DLC coatings [13], however, this bond layer is insufficient when sliding wear takes place in simulated body fluid condition, even at lower contact pressure. This was mainly due to the infiltration of the liquid through the pores and the weakening of the interface due to corrosion processes. The use of a-SiN$_x$:H as an interface layer significantly improved the wear resistance of DLC films in Ringer's solution. By acting as a barrier layer, the a-SiN$_x$:H film reduced the infiltration of the liquid through the film and hence the possibility of interface weakening.

The Open Circuit Potential measurements were used to follow in situ the degradation of DLC-coated surfaces in electrolytic solutions. A drop in the OCP indicated the removal of the DLC layer and the exposure of the active metal to the environment. Moreover, the OCP measured during the tribocorrosion experiments was shown to strongly depend on the cathodic reaction rate on the unworn area; a slower rate of cathodic reaction resulted in lower potential during wear.

The EIS technique was used to assess the effect of sliding wear on the protection efficiency of the DLC films. The delamination of the DLC coating results in a significant decrease of the impedance,

but the preserved high value of the impedance underlines excellent protective properties of the coating system.

The SS/a-SiN_x:H/DLC coating system is very promising for its applications in medical devices and further studies are now in progress.

Acknowledgements

The authors wish to thank Mr. Francis Turcot for his expert technical assistance and Dr. Subhash Gujrathi (Université de Montréal) for the ERD measurements. This work was supported by Medtronic and NSERC of Canada through its university-industry partnership program. We particularly acknowledge Drs. Eunsung Park and Kate Taylor (Medtronic) for stimulating discussions and comments.

References

[1] S. Mischler, A. Spiegel, M. Stemp, D. Landolt, Wear 251 (2001) 1295–1307.
[2] P. Jemmely, S. Mischler, D. Landolt, Tribol. Int. 32 (1999) 295–303.
[3] P. Ponthiaux, F. Wenger, D. Drees, J.P. Celis, Wear 256 (2004) 459–468.
[4] S. Barril, S. Mischler, D. Landolt, Wear 256 (2004) 963–972.
[5] P.E. Sinnet-Jones, J.A. Wharton, R.J.K. Wood, Wear 259 (2005) 898–909.
[6] A.S. Shanbhag, J.J. Jacobs, J. Black, J.O. Galante, T.T. Glant, J. Biomed. Mater. Res 28 (1994) 81–90.
[7] H.F. Hildebrand, J.-C. Hornez, in: J.A. Helsen, H.J. Breme (Eds.), Metals as Biomaterials, John Wiley & Sons, Chichester (UK), 1998, pp. 265–290 (chapter 9).
[8] A. Bendavid, P.J. Martin, C. Comte, E.W. Preston, A.J. Haq, F.S. Magdon Ismail, R.K. Singh, Diamond Relat. Mater. 16 (2007) 1616–1622.
[9] L. Martinu, in: F. Garbassi, E. Occhiello (Eds.), High Energy Density Technologies in Materials Science, Kluwer, Dordrecht, 1989, p. 77.
[10] A. Raveh, L. Martinu, S.C. Gujrathi, J.E. Klemberg-Sapieha, M.R. Wertheimer, Surf. Coat. Technol. 53 (1992) 275–282.
[11] A. Raveh, L. Martinu, H.M. Hawthorne, M.R. Wertheimer, Surf. Coat. Technol. 58 (1993) 45–55.
[12] L. Martinu, A. Raveh, A. Domingue, L. Bertrand, J.E. Klemberg-Sapieha, S.C. Gujrathi, M.R. Wertheimer, Thin Solid Films 208 (1992) 42–47.
[13] R. Snyders, E. Bousser, P. Amireault, J.E. Klemberg-Sapieha, E. Park, K. Taylor, K. Casey, L. Martinu, Plasma Process Polym. 4 (2007) 51–57.
[14] R. Butter, M. Allen, L. Chandra, A.H. Lettington, N. Rushton, Diamond Relat. Mater. 4 (1995) 857–861.
[15] V. Novotny, N. Staud, J. Electrochem. Soc. 135 (1998) 2931–2938.
[16] A. Zeng, E. Liu, I.F. Annergren, S.N. Tan, S. Zhang, P. Hing, J. Gao, Diamond Relat. Mater. 11 (2002) 160–168.
[17] P. Papakonstantinou, J.F. zhao, P. Lemoine, E.T. McAdams, J.A. McLaughlin, Diamond Relat. Mater. 11 (2002) 1074–1080.
[18] M.A.S. Oliviera, A.K. Vieira, M. Massi, Diamond Relat. Mater. 12 (2003) 2136–2146.
[19] H.G. Kim, S.H. Ahn, J.G. Kim, S.J. Park, K.R. Lee, Thin Solid Films 475 (2005) 291–297.
[20] R.S. Lillard, D.P. Butt, T.N. taylor, K.C. Walter, M. Nastasi, Corros. Sci. 39 (1997) 1605–1624.
[21] M. Azzi, J.A. Szpunar, Biomol. Eng. 24 (2007) 443–446.
[22] E.E. Stansbury, R.A. Buchanan, Fundamentals of Electrochemical Corrosion, ASM Int., 2000.
[23] A. Berradja, F. Bratu, L. Benea, G. Willems, J.P. Celis, Wear 261 (2006) 987–993.
[24] Z. Bou-Saleh, A. Shahryari, S. Omanovic, Thin Solid Films 515 (2007) 4727–4737.
[25] C. Liu, Q. Bi, A. Leyland, A. Mattews, Corros. Sci. 45 (2003) 1243–1256.